Characterization of a Geiger-mode Avalanche Photodiode

Christopher W. Maloney

Abstract—**A 32 by 32 array of packaged 100 μm Geiger-mode avalanche photodiodes were tested and characterized. A breakdown voltage of 32 V was measured; at or just above this voltage is where the device should be biased in order to operate in Geiger-mode. The ideal region of the forward biased IV curve resulted in an ideality factor of 1.0 and no recombination/generation region. In addition, IDL code was written to acquire, analyze and reduce an afterpulsing experiment. After looking at the data no afterpulsing was seen in this device. This can be attributed to the fact that there is no recombination/generation region meaning there are a minimal amount of traps in the device.**

Index Terms—**afterpulsing, camera, Geiger-mode APD, LIDAR**

I. INTRODUCTION

GEIGER-MODE avalanche photodiodes (APDs) have been known to be more sensitive than linear-mode APDs and therefore require lower power and less expensive lasers in order to act as a light detection and ranging (LIDAR) imaging detector. A Geiger-mode APD imaging detector that was fabricated at Massachusetts Institute of Technology's (MIT) Lincoln Laboratory has not yet been fully characterized and the capabilities of it are not yet known. By analyzing the behavior of the device, many insightful parameters can be extracted.

II. CAMERA DESIGN AND FABRICATION

One task that needed to be accomplished in order to test and image with the detector was to design and fabricate a light tight camera enclosure. The camera was designed to be light tight, provide external interfaces for all of the connectors on the readout board and be easily accessible for probing of the readout board. SolidWorks was used to design the camera, and gaskets were used along the lid and all connectors on the box to ensure that it was light tight. Figure 1 shows a comparison between the computer aided-design (CAD) camera and the actual fabricated camera. The readout board mounted in the camera can be seen in Figure 2.
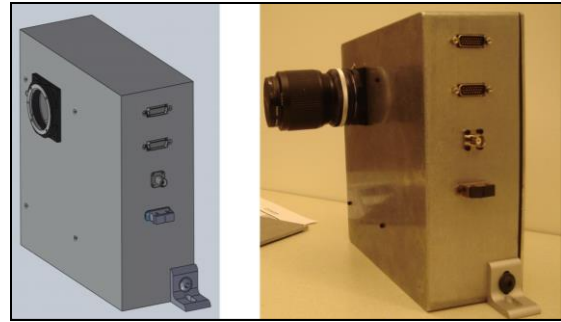
Fig. 1. CAD camera part (Left). Fabricated camera part (Right).

Fig. 2. CAD camera part (Left). Fabricated camera part (Right).

In addition, a separate lid design was needed to accommodate a calibrated diode to be placed at the exact position of the detector in order to measure how many photons penetrate the camera enclosure and are incident on the detector (Figure 3). After careful measurements, a photon flux of 0.0004 photons per microsecond per pixel was determined (sufficient enough for testing and imaging). This was further analyzed to determine where the photons were entering the camera system. It was noticed that the lens assembly on the camera was actually quite heavy and was pulling down on the lens mount creating just enough of a gap to let a very small amount of light enter the camera. This was accounted for and the top of the lens mount was covered with black tape. The camera was now ready to provide a sufficient enclosure for the detector to image and be tested.

C. W. Maloney is with the Rochester Institute of Technology, Rochester, NY 14623 USA (phone: 585-489-9699; e-mail: cwm3854@ rit.edu).
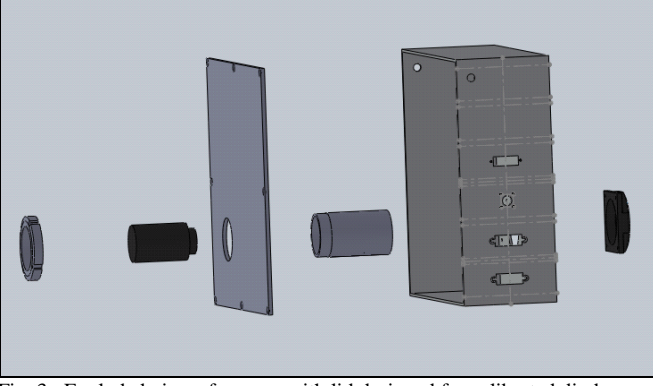
Fig. 3. Exploded view of camera with lid designed for calibrated diode.

III. DIODE IV TESTING

In order to extract certain parameters in the LIDAR device, diodes on a wafer that match the design of those on the LIDAR detector were measured and analyzed using an Agilent 4156B Parameter Analyzer. The diodes measured can be seen in Figure 4.
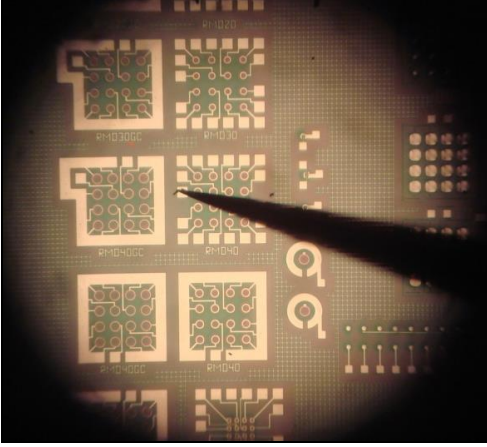
Fig. 4. Diodes measured on a wafer.

Three separate diodes were measured at three different locations on the wafer. All three of the diode IV curves can be seen in Figure 5. This plot shows that all three diodes follow a similar characteristic and it was assumed that all diodes across the wafer share the same trend. From this plot the breakdown voltage extracted was 28 V. In order for the LIDAR detector to operate in Geiger-mode, it must be biased at or just above 28 V. This curve also shows a dark current of approximately 0.1 pA; a very low current measure. The devices measured were approximately 100μm in diameter giving a dark current density of 3.18 nA/cm^2 (area of a circle was used in
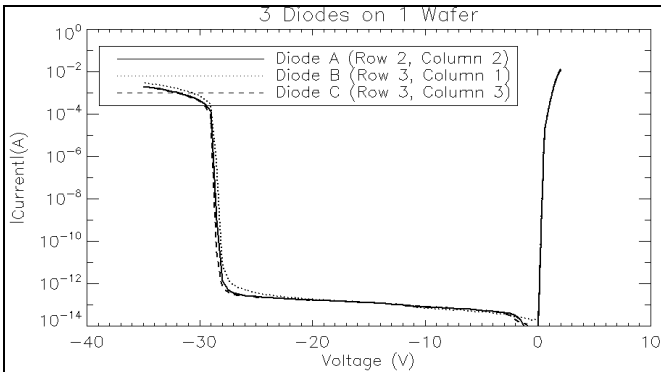
Fig. 5. Measured Reverse Biased Diode IV Curves.

calculation).

In addition, the forward biased diode IV characteristic was also studied. From the plot in Figure 6, it can be seen that the ideal region of the diode is the most dominant and that there is virtually no recombination/generation region in the curve. Using Equation 1, the ideality factor of the ideal region of the diode was calculated to be exactly 1.0. From this, an ideal fit could be calculated and plotted to see the voltage range in which the diode is acting as an ideal diode (Equation 2). In this equation I_o was calculated to be 2.77×10^{-15} A. From this analysis, it can be assumed that there are minimum trap centers in the LIDAR detector since there is almost no recombination/generation region in this diode. The series resistance was also calculated to be on the order of 2 kΩ using equation 3. The difference in voltage between the ideal fit and the actual voltage in the series resistance region of the device is divided by the current at which both of these voltages occur, in order to calculate the series resistance. These devices were design to have high series resistance in order to reduce cross talk between pixels.
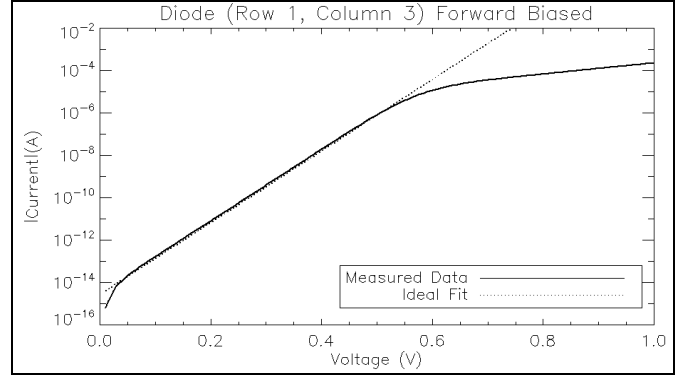
Fig. 6. Measured Forward Biased Diode IV Curve.

$$n = \frac{q}{\left[\ln\left(\frac{I_1}{I_2}\right) \Big/ (V_1 - V_2) \right] \bullet kT} \quad (1)$$

$$I_{ideal} = I_O e^{\frac{qV}{nkT}} \quad (2)$$

$$R_S = \frac{V_{Rs} - V_{ideal}}{I} \quad (3)$$

IV. DARK COUNT RATE VS. BIAS

A dark count is a thermally generated event. Since a Geiger-mode APD is designed to completely avalanche when an event occurs thermally generated events are referred to as dark counts. The dark count rate measures the number of dark counts per seconds, and is analogous to dark current. The calculation of dark count rate is dependent on Poisson statistics and is calculated using Equation 4. The dark count rate in events per second is defined as ρ. N_C is the average number of counts. The number of timing gates N_G can also be viewed as the number of pixels times the number of frames captured. The length of the timing gate in seconds is

represented as τ.

$$\rho = \frac{-\ln\left(1 - \dfrac{N_C}{N_G}\right)}{\tau} \qquad (4)$$

A dark count rate versus bias curve was generated after testing the actual detector, which is a 32x32 array of Geiger-mode APDs. For this test, IDL code was implemented to acquire, analyze and reduce the data. This code was modified to acquire 12,700 frames of data for each bias value, which results in a total number of 13,004,800 gates for each bias value. This was also repeated at various gate width values. Figure 7 shows the dark count rate versus bias plot for a gate width of 800ns. One thing to notice is that the shape of this plot is similar to the reverse bias of the IV curve. There is one difference that the breakdown voltage of the actual detector seems to be around 32 V rather than the 28 V seen in the IV curves. This is most likely due to the fact that these two devices were fabricated on separate wafers during separate runs, which could easily account for a breakdown voltage shift.

V. AFTERPULSING
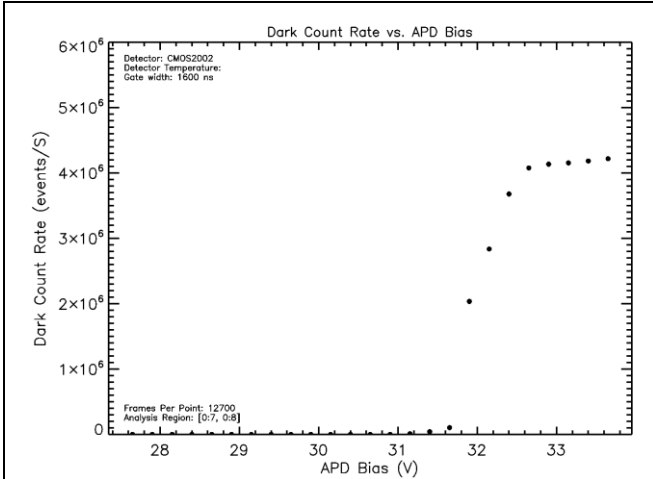
Fig. 7. Measured Dark count rate versus APD bias.

An afterpulsing model was applied and modified to account for this specific LIDAR system [1]. Eq. 5 shows the model that is used to calculate dark count rate (λ) as a function of dead time (t_{dead}). Dead time is the amount of time between gate widths. If this value is too short, one could see an increase in dark count rate due to the release of trapped charge for short dead times. R_{dark} is the measured dark count rate when the detector is not experiencing afterpulsing. The probability that the releasing of a trapped charge will cause a complete avalanche is represented as P_a. N_{ft} represents the number of filled traps and τ_{trap} is the trap lifetime.

$$\lambda(t_{dead}) = R_{dark} + P_a \frac{N_{ft}}{\tau_{trap}} \exp\left(-\frac{t_{dead}}{\tau_{trap}}\right) \qquad (5)$$

Deep level traps, such as sodium are not major contributors to afterpulsing, instead traps with lower activation energies contribute to afterpulsing as seen in Figure 8 (model generated

from Equation 1). Trap lifetimes were calculated from Eq. 6. For this, the activation energy (E_a), and temperature (T) are the only variables for the trap lifetime. This makes the assumption that the trap cross section, the average thermal velocity of carriers and the effective density of states has an overall temperature dependence of T^2 [1].

$$\tau_{trap} = \frac{1}{T^2} e^{E_a/kT} \qquad (6)$$

The experimental data shows no afterpulsing (Figure 9), this can be for a variety of reasons. Either there are no traps in the detector or the trap lifetime is such that it is insignificant to
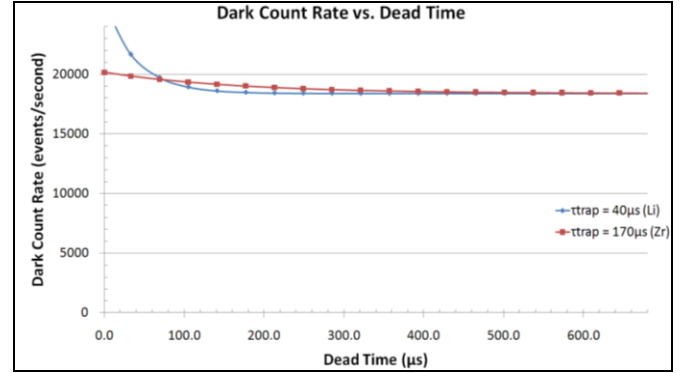
Fig. 8. TheoreticalDark count rate versus Dead Time.

afterpulsing. Trap lifetimes that are too short (< 20 μs) are typically shallow energy level traps and will not be measurable at the minimum dead time achievable with this system. Furthermore, if the trap lifetime is too long (> 500 μs) then the increase in dark count rate will be minimal and not visually apparent on a plot. After looking at the forward biased diode IV curve (Figure 6) it is likely that there are no traps present in this device since there is no recombination/generation region. This would result in no afterpulsing.

VI. CONCLUSIONS

After analyzing the data, a few conclusions can be made.
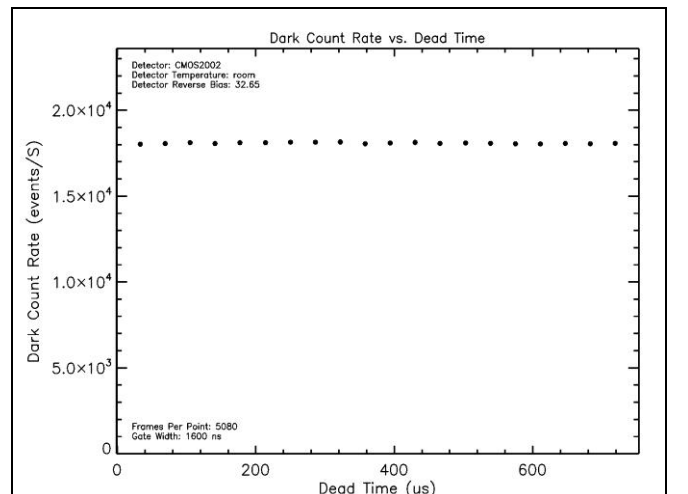
Fig. 9. Measured Dark count rate versus Dead Time.

First, the camera system is light tight and should be able to image outside on a sunny day. Also, it is not possible to assume a breakdown voltage of a device. From wafer to wafer the breakdown voltage seems to vary as seen in the difference between the diodes on the wafer and the packaged diodes. It can be assumed that all diodes on a single wafer have similar breakdown voltages and dark currents as seen in Figure 5. In addition, the diode has been designed carefully and successfully to provide an ideality factor of 1.0 with no recombination/generation region. This made it impossible to see any afterpulsing in the device. Although afterpulsing is not desirable it would have been insightful to see afterpulsing and then analyze the results in order to extract which type of trap is present. RIDL now has IDL code written to test future devices that they will be receiving from MIT in the coming months.

REFERENCES

[1] K.E. Jensen, "Afterpulsing in Geiger-mode avalanche photodiodes for 1.06 μm wavelength" Lincoln Laboratory, MIT 2006.

[2] D. Neamen, "An Introduction to Semiconductor Devices" McGraw Hill 2006.

[3] R.F. Pierret, "Semiconductor Device Fundamentals" Addison-Wesley Publishing Company, Inc. 1996.

[4] B.F Aull,. "3D Imaging with Geiger-mode Avalanche Photodiodes," Optics and Photonics News, 16, 42-46 (2005).

[5] M. Jack, "MBE Based HgCdTe APDs and 3D LADAR Sensors," SPIE, 6542, 2007.

[6] F. Amzajerdian, "Development of Lidar Sensor Systems for Autonomous Safe Landing on Planetary Bodies," 2010.

Christopher W. Maloney was born in Rochester, New York (February 20, 1988) and is a student of microelectronic engineering and physics. Maloney will graduate with a BS degree in microelectronic engineering from Rochester Institute of Technology and with a BS degree in physics from Roberts Wesleyan College in May 2011.

He has worked at National Semiconductor Corporation as a dry etch process engineering co-op. He is currently working for Dr. Don Figer in the Rochester Imaging Detector Laboratory. He has been accepted to a PhD program in microsystems engineering at Rochester Institute of Technology and will start work for Dr. Bruce Smith in the Nanolithography Research Laboratory in June 2011.